Journal of Materials Chemistry A

Accepted Manuscript

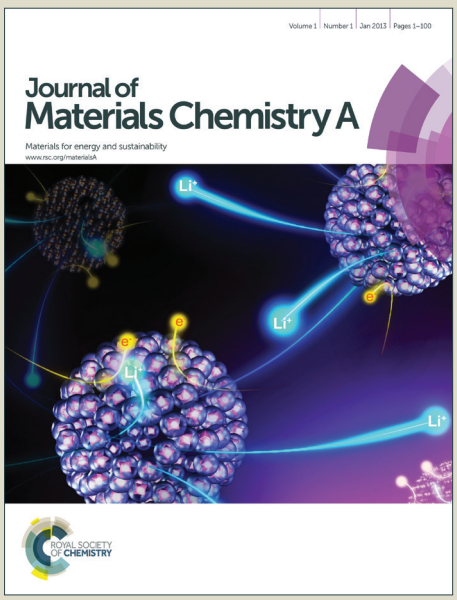

ROYAL SOCIETY OF CHEMISTRY

www.rsc.org/materialsA

Photocatalytic hydrogen production over CdS: Effects of reaction atmosphere studied by *in situ* Raman spectroscopy

Lijing Ma, Maochang Liu, Dengwei Jing, Liejin Guo**

[*] Dr. L. Ma, Dr. M. Liu, Dr. D. Jing, Prof. L.J. Guo
International Research Center for Renewable Energy
State Key Laboratory of Multiphase Flow
Xi'an Jiaotong University, Xi'an, Shaanxi 710049 (P. R. China)
E-mail: ljma@mail.xjtu.edu.cn; lj-guo@mail.xjtu.edu.cn

[**] This work was supported by the National Nature Science Foundation of China (No.50821064, 20906074) and National 863 Program of China (No.2012AA051501).

Abstract

CdS is a well-known efficient photocatalyst for photocatalytic hydrogen production. However, CdS is prone to photocorrosion in the photocatalytic reaction where CdS itself is oxidized by the photogenerated holes. Most of the work reported up to now only focused on the structure of CdS itself. Less attention was, however, paid to the kinetic changes of CdS during photocatalytic reaction, which, in our opinion, is crucial step for its practical utilization. In this report, we developed a facile *in situ* Raman analysis, aiming to clarify the microstructure changes of CdS during the photocatalytic reaction process. In this study, photocatalytic hydrogen production over CdS in Ar or air atmosphere was studied by various techniques besides of the in-situ Raman. With Raman spectrum, a significant increase in surface lattice strain of CdS is observed only when it is exposed to air, while electron-phonon interactions remain the same regardless of the atmosphere. A direct correlation between interfacial crystal lattice and photo-corrosion of sulfide photocatalyst during its photocatalytic hydrogen production was found based on our in-situ Raman investigation. Finding of photo-corrosion of sulfide photocatalyst at its very early stage with our in-situ Raman technique is expected to provide meaningful guidance for the design of active and stable chalcogenide photocatalysts, which, however, cannot be achieved by traditional characterizing techniques.

Keywords: Hydrogen production; CdS; Raman spectrum; reaction atmosphere

1. Introduction

Photocatalytic decomposition of water over semiconductors provides an ideal way for hydrogen production.[1-7] The key of this technique is to synthesize photocatalysts with high photoactivity and stability but of low cost. As an important direct-band-gap (2.5 eV) semiconductor, cadmium sulfide (CdS) has been extensively studied for potential applications ranging from light-emitting diodes, optical devices, and photocatalysis.[8] However, there is an inherent drawback for CdS-based photocatalysts, *i.e.*, photocorrosion where CdS itself is oxidized by the photogenerated holes.[9] It is believed that photo-corrosion have occurred for these chalcogenide photocatalysts when their activity become irreversibly decreased even with re-addition of sacrificial agent. Various efforts have been made to improve the stability of CdS and remain its high photoactivity, as reported in our previous work.[10-12] It has also been reported that photoetching of CdS leading to an enhancement of the photocatalytic activity by reduction of surface recombination centers. The enhanced activity was also attributed to the increased surface roughness and specific surface area.[13] Generally, it was often found that CdS with similar crystal structure showed obviously different activity when the reaction atmosphere is slightly changed. For example, when oxygen is introduced, the photoactivity could be dramatically lowered due to the possible acceleration of the photocorrosion process. Up to now, most of the work reported only focused on the structure of CdS itself. Less attention was, however, paid to the kinetic changes of CdS during photocatlytic reaction. In our opinion, finding of photo-corrosion of sulfide photocatalyst at its very early stage is the first and important step toward the design of stable sulfide photocatalyst. However, less work has been done in this respect due mainly to the lower resolution of traditional techniques such as XRD, XPS, etc. No convincing changes of the micro structure of CdS can be found by these techniques even after reaction of several hours and when the activity become obviously decrease.

It is well known that optical phonons significantly affect the carrier relaxation process and emission efficiency in semiconductor nanostructures, which can be probed by Raman scattering. In specific, Raman scattering can probe the longitudinal optical

(LO) and the transverse optical (TO) phonons, offering a useful means to investigating, with a Spectral level resolution, the crystalline quality, strain and electron-phonon interaction in semiconductor nanostructures.[14] Herein, we developed a facile *in situ* Raman analysis, aiming to clarify the microstructure changes of CdS, the role of O_2, and thereby photo-corrosion process during photocatalytic reactions. The work is expected to provide meaningful guidance for the design of active and stable chalcogenide photocatalysts, which, however, cannot be achieved by traditional characterizing techniques.

2. Experimental

2.1. In situ Raman experiment

CdS was used as purchased. All the reagents were of analytical grade and used without further purification. The flowchart for the In situ Raman experiment is schematically shown in Fig.1. Photocatalyst CdS (0.05 g) was dispersed in a quartz reaction cell containing aqueous solution (4 mL) of Na_2S (0.168 g) and Na_2SO_3 (0.072 g) as electron donors. Argon or air was purged through the cell for 10min before reaction. Then the quartz reaction cell was sealed. As a control experiment, the quartz reaction cell was sealed with Ar/O_2 mixture containing 20% volume fraction of O_2, or in vacuum. The photocatalysts were irradiated with visible light from a XD-300 high brightness gold light source. The Raman measurements were performed at room temperature over a Jobin-Yvon LabRam HR 800 micro-Raman system, equipped with a liquid-N_2-cooled detector. A Melles-Griot air-cooled Ar ion laser with 514.5 nm excitation wavelength was used. The excitation line had its own interference filter (for filtering out the plasma emission) and a suitable Raman notch filter (for laser light rejection). The laser power was 30mW. All measurements were taken with a 600 $g \cdot mm^{-1}$ grating and a confocal microscope of 100μm aperture via an optical microscope in a back scattering geometry. The frequency position of crystalline Si Raman line at 520 cm^{-1} was used to calibrate the system in the present study.

2.2. Characterization

X-ray diffraction (XRD) patterns of CdS before and after reaction were confirmed by an X'Pert PRO diffractometer using Cu Ka irradiation. Diffuse reflectance UV-vis spectra were measured on a Hitachi U-4100 instrument equipped with a lab-sphere diffuse reflectance accessory. The crystallite morphologic micrograph was observed by a JEOL JSM-6700F field emission scanning electron microscopy (SEM) and a transmission electron microscope (TEM) FEI Tecnai G2F30 S-Twin. Photoluminescence (PL) spectra were recorded with the excitation wavelength of 360 nm using Xe lamp in the range of 350-900 nm at the room temperature. X-ray photoelectron spectroscopy (XPS) was measured on a Shimadzu ultra DLD instrument. For photocatalytic hydrogen evolution, 0.2 g photocatalyst powder was dispersed by a magnetic stirrer in a side irradiated photocatalytic reactor containing aqueous solution (200 mL) containing Na_2S (2.0 g) and Na_2SO_3 (9.6 g) as electron donors. The reaction cell was connected to a gas circulation system and the hydrogen evolved was analyzed by an on-line TCD gas chromatograph (NaX zeolite column, argon as carrier gas) The photocatalysts were irradiated with visible light from a 300 W PLS-SXE300 Xe lamp and the UV part of the light was removed by a cut-off filter ($\lambda > 420$ nm).

3 Results and Discussion

3.1 Characterization of CdS before and after photocatalytic reaction with traditional techniques

The XRD patterns of CdS before and after photocatalytic reaction under air and Ar, respectively, were shown in Fig.2. The intensive peaks from 20^o to 60^o indicate that all three samples are typical hexagonal CdS. From the XRD results after photocatalytic reaction under air, it seemed that the crystalline phase of CdS was not affected by the presence of air gas. It is assumed that photo-corrosion should occur for CdS after photocatalytic reaction of 8h. In this case, the crystallinity of CdS shoud be lowered leading to decreased diffraction intensity. This can also be demonstrated by the fact that CdS reacting under Ar has higher diffraction intensity than CdS reacting under air. We also examined the SEM and TEM images of CdS before and after photocatalytic

reaction under Air and Ar, respectively. The representative results are shown in Fig.3 and Fig.S1 in ESI. Clearly, all three samples occupied almost similar spherical shape, regardless of photocatalytic reactions as well as the reaction atmosphere. The decrease of crystallinity of CdS was also found in agreement with XRD results.

To evaluate the chemical states of the CdS, XPS analyses were conducted over the samples before and after photocatalytic reaction under Air and Ar, respectively (Fig. 4). No noticeable changes in binding energy in terms of both Cd and S elements could be found, indicating well maintained elemental chemical states during the reactions even in the presence of oxidative air atmosphere. In fact, the use of Na_2S and Na_2SO_3 as electron donors that has been considered as one of the important methods to improve the stability of CdS. [10-12]

In addition, we also checked the optical properties of these samples after the photoreaction using UV-Vis spectra. As shown in Fig.5, the sharp absorption with an onset around 550 nm for all CdS samples indicated pure band-gap transition of electrons from the valance band to the conduction band of CdS. It is also found relatively increased absorption after 550 nm on CdS samples after the photoreactions. Combined with XRD and XPS analyses shown in Fig. 2 and Fig. 4, it is reasonable to attribute the changes to the remaining absorbed S^{2-} or SO_3^{2-} after reaction. As reported in our previous study and reference wherein, S^{2-} would react with excess elemental S to form yellow polysulfide ions, such as S_2^{2-} and S_4^{2-}, which would affect the optical absorption of the photocatalyst in the reaction solution. [15] This can be avoided by adding SO_3^{2-} to the reaction medium, to form a transparent solution of the $S_2O_3^{2-}$. On the other hand, photocorrosion often means the possible formation of elemental S.[9] The decrease of the relative absorption intensity before 550 nm and the strong background absorption after 550 nm for CdS after reaction under both Ar and air, could therefore be related to the absorbed S^{2-} or SO_3^{2-} remaining after reaction though CdS have been washed repeatedly and dried before UV-Vis spectra. It is worthy pointing out that the missing signal of corresponding S (IV) in XPS spectra should be due to the resolution limitation as very small amount absorption of S^{2-} or SO_3^{2-} on CdS surface.

Photoluminescence spectra for CdS samples before and after photocatalytic reaction under Air and Ar, respectively, were also recorded as in Fig.6. Strong emission peak around 425 nm could be observed for all the CdS samples, and the PL peak intensities increased after photocatalytic reaction. The sharpness of the peak could be attributed to the narrow distribution of the particles and no notable peaks attributed to surface states could be observed.[16,17] Particularly, emission for CdS after photocatalytic reaction under Air showed a prominent increase than its counterpart before reaction. The energy corresponds to 450 nm emission is 2.8 eV, higher than the band-gap energy calculated from the extinction spectrum. It can be understood that the peaks do not originate from defect sites or surface states. The enhancement of photoluminescence has been attributed to the increase of radiative recombination and decrease of non-radiative recombination.[18] Our PL results showed that the photocatalytic reactions in air could lead to stronger photoluminescence than in Ar. Stronger photoluminescence often indicates increased number of surface states which often acts as recombining center of photo-generated charges and therefore leads to lower activity of the photocatalyst.[10] These PL results were in agreement with the photocatalytic hydrogen production as will be shown in the following part.

Photocatalytic hydrogen tests over CdS under Ar and air have been conducted. Here, to exclude the possible contribution from Pt, bare CdS without Pt loading was used.[19] Hydrogen evolution rates under Ar and air, respectively, were plotted against the reaction time, as shown in Fig.7. It was found that both reaction showed a *ca.* 3 h activation period and then exhibited a quite stable hydrogen production. Hydrogen production under Ar is much higher than under air. Obviously, photocatalytic hydrogen production in air is not favorable. The reason for the low photocatalytic rate was supposed to be the introduction of O_2, which is considered detrimental to CdS. However, the explicit role of O_2 along with experimental proofs remains a great challenge to date.

3.2. *In situ* Raman characterization

As aforementioned, Raman scattering spectra can give useful information featured on photon-crystalline interaction by evaluating the spectral peak position and the

spectral width of its Raman spectra, which cannot be obtained by XRD.[20] To this end, we developed a facile photocatalytic system equipped with *in situ* Raman analysis (see Fig.1 for detail). Fig. 8 shows the obtained Raman spectra against irradiation time when the reaction was carried under air or Ar. Lorentzian line shape is fitted to the Raman spectrum from which the peak position and Full Width at Half Maximum (FWHM) have been obtained. It is known that A1, E1, and E2 symmetry modes are allowed for hexagonal CdS with space group of C46v/C63mc.[21] As a control experiment, the quartz reaction cell was sealed with Ar/O_2 mixture containing 20% volume fraction of O_2, or in vacuum (ESI, Fig.S2). As shown in Fig.S2a, the 1LO Raman shift and FWHM for CdS reacting under Ar/O_2 mixed atmosphere showed very similar curves to that under air. It indicates that N_2 and CO_2 in air would not obviously affect the Raman spectral of CdS during its photocatalytic reaction. The possible influence of N_2 and CO_2 from air can thus be excluded. On the other hand, as shown in Fig.S2b, Raman shift and FWHM for CdS reacting under vacuum showed generally similar trend to that under Ar. Although there is certain difference, it is assumed that the gas pressure should not the decisive factor affecting our in-situ Raman monitoring.

In Fig.8a, the peak around 300 cm^{-1} is the 1LO (longitudinal optical) phonon resulting from the A1 mode of the Cd-S bond vibration.[22] The peak at ca. 600 cm^{-1} is 2LO of CdS. The third harmonic at 900 cm^{-1} is very weak for all curves. These Raman spectra are essentially independent of the electron donors in the reaction solution. No peaks belonging to pure $CdSO_3$ and CdO representing the oxidation products of CdS could be found.[23] Some small peaks are supposed to be related to the Raman scattering peak of Na_2S and Na_2SO_3. Obviously in Figure 8, some peaks located around 500 cm-1 appeared after about 1 h and the intensity increased as the reaction proceeded. It has been reported that the CdO has a weak Raman peak at ca. 500 cm^{-1} [24]. It is thus inferred that in our case, the existence and continuous growth of 500 cm^{-1} peak should be related to the substitution of some surface S atoms by O which cannot be detected by XRD due to its lower resolution. As shown in Figure 8a and 8c, 500 cm^{-1} Raman peak was greatly suppressed for CdS reacting under Ar than in air

especially before 100mins of reaction. This is another evidence for the partial oxidation of CdS surface. The shift of the Raman peak to higher wave numbers and increase of lattice stress should also be attributed to the replacement of sulphur atoms by the lighter oxygen atoms. It is an indication of the photo-corrosion at its very early stage which cannot be found by traditional XRD technique.

To understanding the lattice change of CdS, we also summarized the peak shift and FWHM in Fig.8b. The position of 1LO peak is slightly shifted to lower wave numbers with respect to original CdS (305 cm^{-1}). Raman peak for 1LO was 296.7 cm^{-1} before light irradiation, but it became 300.5 cm^{-1} after 5h irradiation. There is an almost lineal relationship between Raman shift and reaction time, indicating the successive shift of 1LO peak. On the contrary, the FWHM undergoes almost lineal decrease and then a sharp increase.

The narrowing of the 1LO peak has been connected to the lattice stress. It has been reported that CdO nanolayer with thickness of 2 nm showed a 310 cm^{-1} Raman peaks, which will rapidly shift to lower wavenumber of 278 cm^{-1} and then 256 cm^{-1} for CdO with thickness of 7 nm and 150 nm, respectively.[25] We thus attributed the increase of wavenumbers of 1LO for CdS and its narrowing to the possible formation of Cd-O that cannot be detected by XRD.

Similar phenomenon can also be observed over the sample reacted under Argon gas (Fig.8, c and d). As shown by Fig. 8c, the 1LO showed no obvious changes in position. The FWHM also showed much smaller decrease with reaction time, compared to that under air gas. The optical phonon behaviors are related to the strain, crystalline quality, and exciton-LO phonon coupling in CdS crystal structures. The strain Δc/c associated with a lattice elongation of the c-axis can be calculated using the following equation,[21,26]

$$\Delta\omega/\omega_0 = (1 + 3\Delta c/c)^{-\gamma} - 1 \quad (1)$$

where $\Delta\omega$ is the 1LO phonon energy shift compared to its bulk value ω_0 and γ is the Grüneisen parameter (γ = 1.1 for CdS). Here, ω_0 is chosen to be 300 cm^{-1} corresponding to the A1 mode of the Cd-S bond vibration in bulk CdS.[21,22] For CdS reacting under air and Ar, respectively, we obtained $\Delta c/c$ versus reaction time, as

shown by Fig.9a. It seemed that CdS reacting in inert gas underwent a much lower strain. However, a lineal increase in strain can be found for CdS reacting under air. I_{2LO}/I_{1LO} ratio has been suggested to be a measure of the strength of the electron-phonon interaction.[27] It can be seen from Fig. 9b that the 2LO-to-1LO intensity ratio increased with the reaction time for both CdS reacting under Ar and Air and the two showed similar tread of change with time. The change in the electron-phonon coupling could arise not only from the changes in the size but also from the change in the structure. The electron-phonon coupling in bulk cubic-CdS has been found to be much lower than that in hexagonal-CdS because of the difference in the symmetries of LO phonons as well as that in the nature of the interband transitions in the two phases.[28,29] The present results most possibly suggest an increase in electron-phonon interaction as a function of reaction time for both reaction under Air and Ar.

Taken all, it can be seen that during photocatalytic hydrogen production, either under air or Ar, there was the increase of lattice stress and electron-phonon interaction for CdS. However the strain and lattice stress increased more prominently for CdS reacting under air. Change of electron-phonon interaction is similar for CdS reacting either under air or Ar. Based on our results, the increased crystal lattice stress during the photoreaction in the presence of air could be ascribed to the enhanced interaction between absorbed O_2 and the surface of photocatalyst, in a physical or/and in a chemical way, which, in turn, gave rise to the decreased activity. Although the nature of such interaction needs further in-depth investigation, our results indicates at least that increase in strain and lattice stress could be the indication of the beginning of the photocorrosion of sulfide photocatalyst at its very early stage which however cannot be detected by other traditional techniques such as XRD. These physical factors should therefore be paid more attention in future study for the development of a stable chalcogenide photocatalyst.

4. Conclusion

CdS-based chalcogenides are very promising materials for photocatalytic applications.

However, inherent instability during photocatalytic reactions greatly limits their practical utilization. In this study, we have investigated the microscale structural properties of CdS before and after photocatalytic reaction. No obvious changes could be found for CdS after photocatalytic reaction, based on structural characterizations (i.e. XRD, XPS, SEM). However, hydrogen production under Ar was found to be much higher than under air. Photo-corrosion was expected to occur over sulfide photocatalyst during its photocatalytic hydrogen production, which cannot be clearly manifested by above characterizations. To overcome this problem ~~this end~~, we developed a facile photocatalytic system equipped with *in situ* Raman analysis to monitor the microscopic changes of CdS during photocatalytic reaction under Ar and air, respectively. Both the increase of lattice stress and electron-phonon interaction for CdS reacting either under air or Ar was found by analyzing in situ Raman results. The lattice stress was found to increase more prominently for CdS reacting under air. Significant increment of lattice stress resulting from the interaction between adsorbed O_2 and CdS, which could not be resolved by traditional characterization, was observed. It was concluded that photo-corrosion could result in lattice stress increase of CdS which could be precisely detected by Raman spectrum. We believe that our finding is valuable for the prediction of photo-corrosion at its very early stage and our study is expected to provide useful information for the development of highly active and stable sulfide photocatalyst in future study.

Acknowledgment

The authors gratefully acknowledge the financial supports from the National Natural Science Foundation of China (Nos. 21276206, 51422604) and National 863 Program of China (No.2012AA051501).

References

[1] M.Yang, N. Zhang, M. Pagliaro and Y. Xu, *Chem. Soc. Rev.* 2014, **43**, 8240-8254.

[2] N. Zhang, R. Ciriminna, M. Pagliaro and Y. Xu, *Chem. Soc. Rev.* 2014, **43**, 5276-5287.

[3] C.Han,M.Yang, B. Weng and Y. Xu, *Phys. Chem. Chem. Phys.* 2014, **16**, 16891-16903

[4] N. Zhang, Y. Zhang and Y. Xu, *Nanoscale* 2012, **4**, 5792-5813.

[5] Y.H.Zhang, N. Zhang, Z. Tang and Y. Xu, *Chem. Sci.*, 2012, **3**, 2812-2822.

[6] C. Han, M.-Q. Yang, N. Zhang and Y. Xu, *J. Mater. Chem. A*, 2014, **2**, 19156-19166.

[7] L. Zhang, D.W. Jing, X.L. She, H.W. Liu, D.J. Yang, Y. Lu, J. Li, Z.F. Zheng and L.J. Guo, *J. Mater. Chem. A* 2014, **2**, 2071-2078.

[8] D.W. Jing, L.J. Guo, L. Zhao, H. Liu, K. Zhang, X.M. Zhang, *Int. J. Hydrogen Energy* 2010, **35**, 7087-7097.

[9] M. Ashokkumar, *Int. J. Hydrogen Energy* 1998, **23**, 427.

[10] D.W. Jing and L.J. Guo, *J. Phys. Chem. B* 2006, **110**, 11139-11145.

[11] M.C. Liu, L.Z. Wang, G.Q. Lu, X.D. Yao and L.J. Guo, *Energy Environ. Sci.* 2011, **4**, 1372-1381.

[12] M.C. Liu, D.W. Jing, Z.H. Zhou and L.J. Guo, *Nat. Commun*. 2013, **4**, 2278.

[13] Y.X. Li, J. Du, S.Q. Peng, D. Xie, G.X. Lu and S.B. Li, *Int. J. Hydrogen Energy* 2008, **33**, 2007-2013.

[14] J.Y. Zhang, X.Y. Wang, M. Xiao, L. Qu and X. Peng, *Appl. Phys. Lett.* 2002, **81**, 2076-2078.

[15] D.W. Jing, L. Jing, H. Liu, S.Yao and L.J. Guo, *Ind. Eng. Chem. Res.* 2013, **52**, 1992-1999.

[16] L. Cao, Y.M. Miao, Z.B. Zhang, S.S. Xie, G.Z. Yang and B.S. Zou, *J. Chem. Phys.* 2005, **123**, 024702.

[17] Z.Q. Wang, J.F. Gong, J.H. Duan, H.B. Huang, S.G. Yang, X.N. Zhao, R. Zhang and Y.W. Du, *Appl. Phys. Lett.* 2006, **89**, 033102.

[18] S.H. Shen, L. Zhao, Z.H. Zhou, and L.J. Guo, *J. Phys. Chem. C* 2008,**112**,16148-16155.

[19] Y.H. Li, J. Xing, Z.J. Chen, Z. Li, F. Tian, L.R. Zheng, H.F. Wang, P. Hu, H.J. Zhao and H.G. Yang, *Nat. Commun*. 2013, **4**, 2500.

[20] X.X. Yang, Z.F. Zhou, Y. Wang, R. Jiang, W.T. Zheng and C.Q. Sun, *J. Appl. Phys.* 2012, **112**, 083508.

[21] K.Y. Lee, J.R. Lim, H. Rho, Y.J. Choi, K.J. Choi and J. G. Park, *Appl. Phys. Lett.* 2007, **91**, 201901.

[22] I.C. Chen, C.L. Weng, C.H. Lin and Y.C. Tsai, *J. Appl. Phys.* 2010, **108**, 083530.

[23] A. Ashrafi and K. Ostrikov, *Appl. Phys. Lett.* 2011, **98**, 133119.

[24] S.A. Mayén-Hernández, G. Torres-Delgado, R. Castanedo-Pérez, J.G. Mendoza-Alvarez and O. Zelaya-Angel, *Mater. Chem. Phys.* 2009, **115**, 530.

[25] L. Lu, X.L. Xu, W.T. Liang and H.F. Lu, *J. Phys. Condens. Matter.* 2007, **19**, 406221.

[26] J.H. Kim, H. Kim, H. Rho, Y.J. Choi and J.G. Park, *J. Phys. D*, 2014, **47**, 135104.

[27] J.J. Shiang, S.H. Risbud and A.P. Alivisatos and J.J. Shiang, *J. Chem. Phys.* 1993, **98**, 8432-8442.

[28] A. Gichuhi, B.E. Boone, C. Shannon, *J. Eelectroanal. Chem.* 2002, **522**, 21-25.

[29] V. Sivasubramanian, A.K. Arora, M. Premila, C.S. Sundar and V.S. Sastry, *Physica E* 2006, **31**, 93-98.

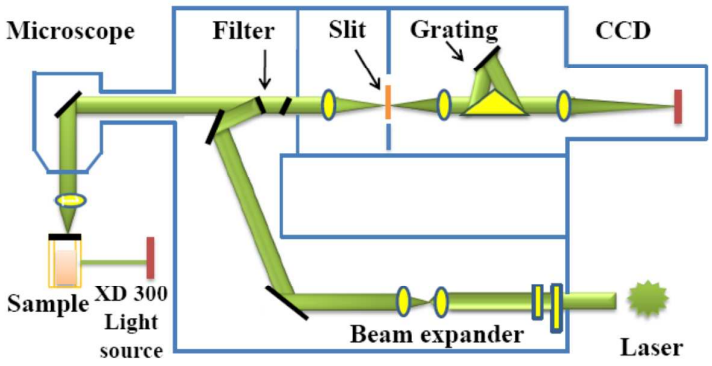

Figure. 1 Schematic representation of the in situ Raman experimental set-up.

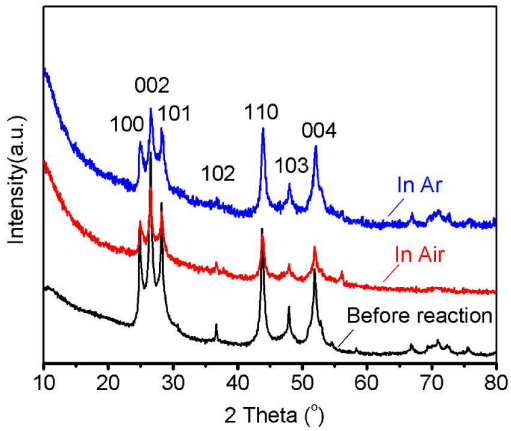

Figure 2 XRD patterns of CdS before and after photocatalytic reaction under air and argon (Ar).

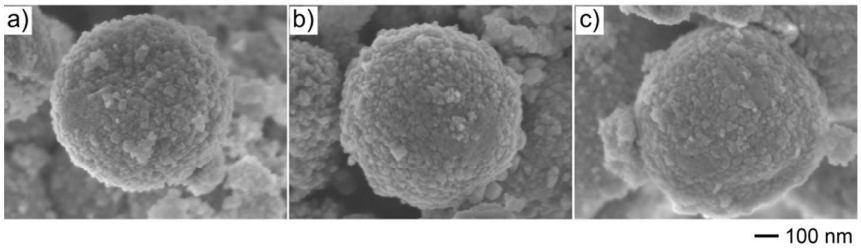

Figure 3 SEM images of CdS before (a) and after photocatalytic reaction under air (b) and Ar (c). Scale bar is 100nm and applies to (a)-(c).

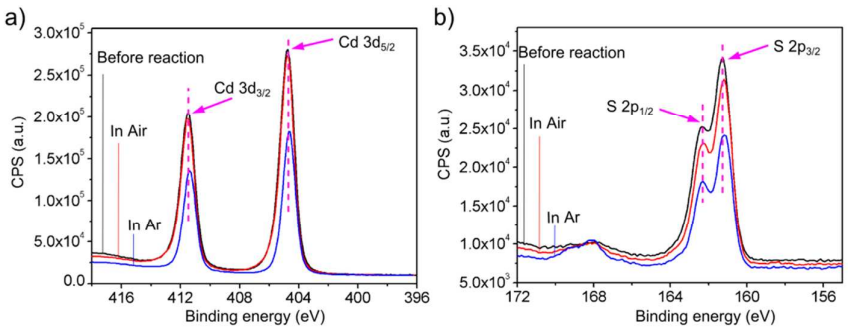

Figure 4 XPS spectra of (a) Cadmium 3d and (b) Sulfur 2p of CdS before and after photocatalytic reaction under Air and Ar.

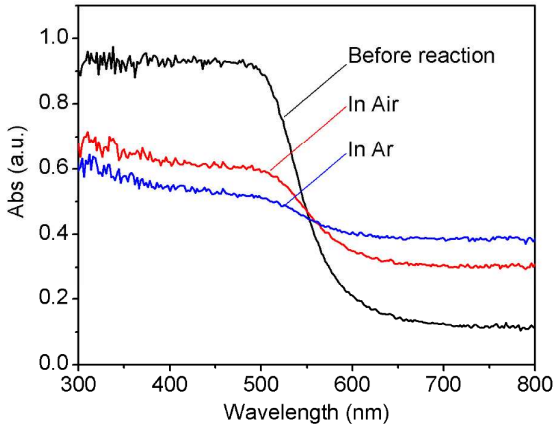

Figure 5 UV-vis spectra of CdS before (black line) and after photocatalytic reaction under Air (red) and Ar (blue).

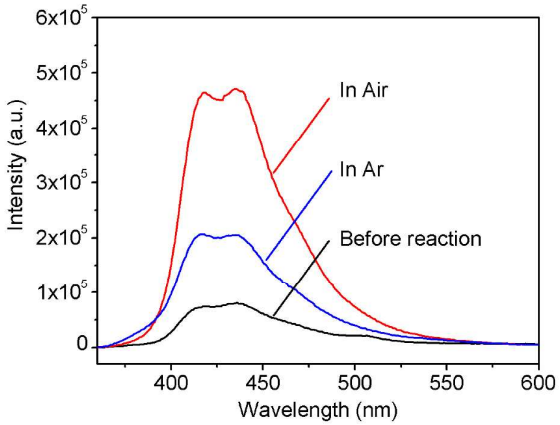

Figure 6 Photoluminescence PL spectra (360 nm excitation) of CdS before and after photocatalytic reaction under Air and Ar.

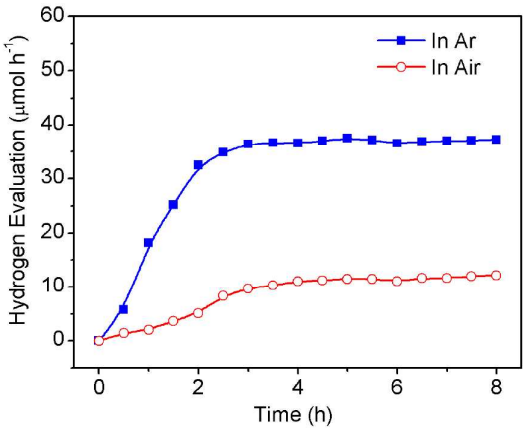

Figure 7 Hydrogen evolution rates of CdS under air and Ar atmosphere, respectively.

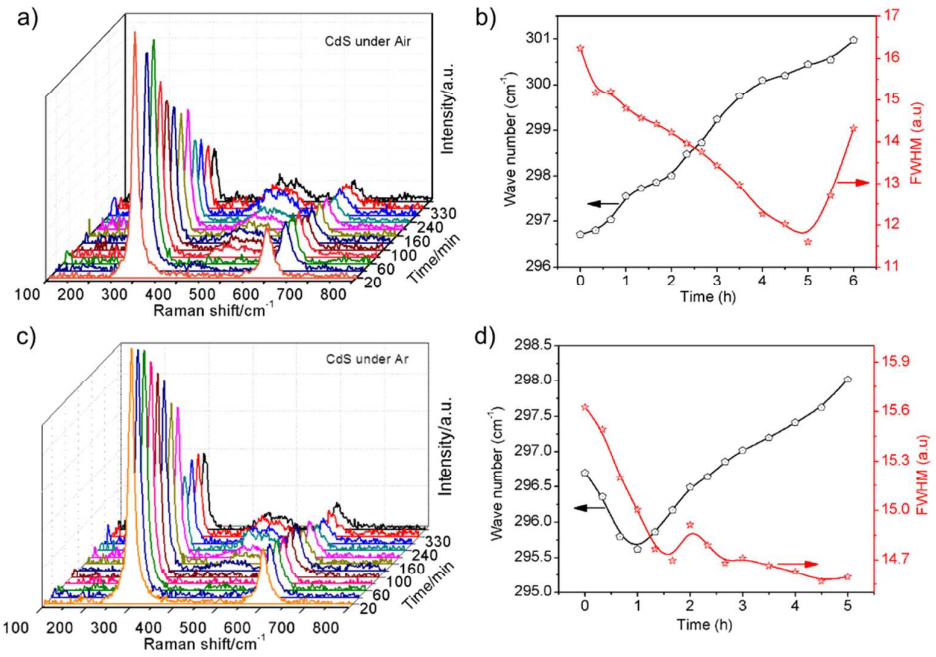

Figure 8 Photocatalytic experiments with in situ Raman monitoring. (a) In-situ Raman spectra of CdS reacting under air, (b) Corresponding Raman shift and FWHM of CdS 1LO peak reacting under air, (c) In-situ Raman spectra of CdS reacting under Ar, (d) Corresponding Raman shift and FWHM for 1LO peak of CdS reacting under Ar.

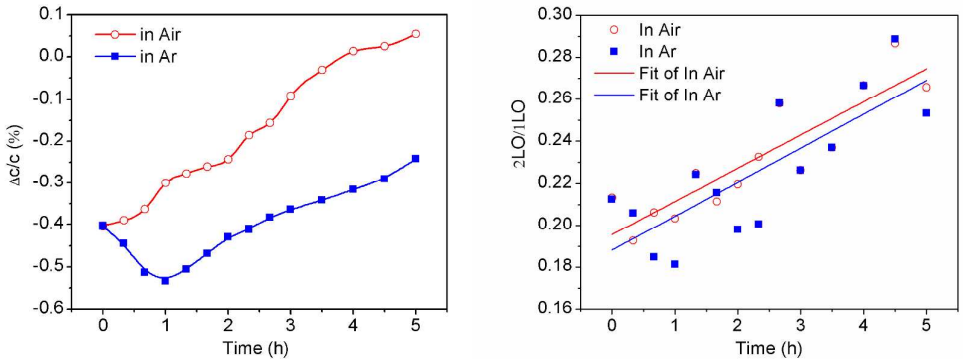

Figure 9 Time dependence of (a) the lattice strain (Δc/c) and (b) 2LO/1LO peak ratio for CdS during photocatalytic reaction under air and Ar atmosphere, respectively.